World Journal of Environmental Biosciences
Available Online at: **www.environmentaljournals.org**

Volume 15, Issue 3: 94-101

https://doi.org/10.51847/hYNO1keXro

ISSN 2277- 8047

Machine Learning and Spatial Statistical Modeling of Urban Heat Islands under Climate Change Scenarios

Leonel Coyla-Idme[1]*, Vladimiro Ibañez-Quispe[1], Jose-Panfilo Tito-Lila[1], Juan Reynaldo Paredes-Quispe[1]

[1]Universidad Nacional del Altiplano de Puno, Puno, Peru.

ABSTRACT

Urban heat islands intensify thermal exposure in cities by concentrating heat in dense built environments, reducing nocturnal cooling, and amplifying the effects of regional climate warming. This study compares machine learning and spatial statistical approaches for predicting current urban heat island intensity and projecting mid-century changes under climate change scenarios. The objective is to evaluate whether predictive accuracy, spatial inference, and climate adaptation relevance can be improved through a combined modeling strategy. The analysis uses a 30-m resolution empirical urban climate dataset for a 100 km² metropolitan study area. Land surface temperature, vegetation, impervious surface fraction, building density, albedo, road density, population density, and socioeconomic indicators were assembled for the summer 2023 baseline. Statistically downscaled CMIP6-based projections were incorporated for 2050 under SSP2-4.5 and SSP5-8.5. Four models were implemented and compared: Random Forest, XGBoost, Spatial Error Model, and Geographically Weighted Regression. Model performance was assessed using spatial k-fold cross-validation, while residual spatial dependence was examined using Moran's I diagnostics. Variable importance, spatial coefficient patterns, and uncertainty intervals were used to compare prediction-oriented and inference-oriented outputs. The results indicate that XGBoost achieved the strongest predictive performance, followed by Random Forest, Geographically Weighted Regression, and the Spatial Error Model. Machine learning models captured nonlinear interactions among vegetation, building density, impervious surface, and albedo, whereas spatial statistical models more effectively reduced residual spatial autocorrelation. Mid-century projections indicated an increase in mean urban heat island intensity of 1.2°C under SSP2-4.5 and 2.8°C under SSP5-8.5. The study is limited by its single metropolitan study area, simplified climate downscaling, and static treatment of urban morphology in future projections. Nevertheless, it provides a transparent empirical framework for comparing predictive machine learning with spatially explicit statistical inference. Its originality lies in systematically linking model comparison, residual spatial diagnostics, and scenario-based urban heat projections for adaptation-oriented urban climate analysis.

Keywords: *Urban heat island, Machine learning, Spatial statistics, Climate change scenarios, Random forest, Geographically weighted regression*

Corresponding author: Coyla-Idme
e-mail ✉ lcoyla@unap.edu.pe
Received: 17 July 2026
Accepted: 29 August 2026

INTRODUCTION

Urban heat islands are produced when built surfaces, compact morphology, reduced vegetation, anthropogenic heat, and altered radiative properties raise urban temperatures relative to surrounding non-urban areas. Systematic reviews of UHI drivers show that land cover composition, surface materials, urban geometry, and vegetation availability jointly shape the intensity and persistence of urban thermal anomalies (Deilami *et al*., 2018). Satellite-based land surface temperature studies have become especially important because they allow heat patterns to be mapped across large urban areas at fine spatial resolution (Zhou *et al*., 2019). Evidence from major Chinese cities further shows that surface UHI trends vary across space and time as urban expansion, vegetation loss, and climatic background conditions interact (Yao *et al*., 2017).

Climate change increases the planning relevance of UHI analysis because background warming can convert existing hot spots into zones of recurrent heat stress(Fischer *et al*., 2024; García *et al*., 2024). Diagnostic modeling of daily maximum UHI intensity in European cities has shown that synoptic conditions and urban structure jointly regulate the magnitude of heat accumulation (Theeuwes *et al*., 2017). Recent climate-model applications for French cities demonstrate that regional climate simulations can represent urban heat patterns, but their usefulness for local planning depends on spatial detail and urban parameterization (Michau *et al*., 2023). Future-oriented UHI projection studies also suggest that warming scenarios can amplify intra-urban thermal inequality when existing built-form contrasts remain unchanged (Ni *et al*., 2025).

Machine learning has become increasingly attractive for UHI modeling because urban thermal responses are often nonlinear, scale-dependent, and interaction-rich. Random Forest applications have been used to model land surface temperature and identify dominant urban characteristics, while XGBoost and SHAP-based approaches have improved interpretation of complex predictor effects (Li, 2022; Oukawa *et al*., 2022; Wang *et al*., 2022). Studies of urban form and heat resilience show that interpretable machine learning can reveal threshold behavior in vegetation, density, and surface material variables that is difficult to capture with linear models alone (Liu *et al*., 2024). However, prediction-oriented algorithms may still leave spatially structured residuals when the spatial dependence of heat processes is not explicitly modeled.

Spatial statistical models offer a complementary strategy because they address spatial autocorrelation, spatial heterogeneity, and local coefficient variation in environmental data (Ba *et al*., 2025; Pop & Stan, 2025). Prior UHI studies have used spatial regression, geographically weighted regression, and 3D urban-form analysis to estimate how parks, land use, tree shade, and buildings influence urban heat patterns (Dai *et al*., 2018; Zhao *et al*., 2018; Park *et al*., 2021). Spatial regression applications across East Asian metropolises confirm that land-use impacts on land surface temperature differ across cities and spatial contexts (Chen *et al*., 2025). This study therefore asks which modeling approach better predicts UHI intensity, how spatial dependence alters interpretation, and how current UHI patterns may change under SSP2-4.5 and SSP5-8.5 by mid-century (Baz *et al*., 2024; Ratnadevi *et al*., 2024).

literature review

Earlier UHI research established that remotely sensed thermal imagery can connect physical urban form to observed surface temperature patterns. A Nanchang study linked land surface temperature to social-ecological variables, demonstrating that UHI intensity is not only a biophysical problem but also an urban systems issue (Zhang *et al*., 2017). Global-scale satellite analysis has shown that vegetation exerts strong control over surface UHI variability, although the strength of that control depends on climatic and urban extent definitions (Chakraborty & Lee, 2019). Work on urban extent discrepancy further indicates that methodological choices in defining cities can alter estimated UHI intensity across large samples of cities (Yang *et al*., 2023).

Machine learning studies have advanced UHI modeling by improving prediction and enabling nonlinear interpretation. Random Forest has been used to compare fine-scale urban heat modeling against multiple linear regression, showing stronger performance when spatially complex predictors are included (Oukawa *et al*., 2022). Machine learning prediction of land use, land cover, and land surface temperature change in Ahmedabad illustrates how urban growth and surface heat can be modeled jointly in rapidly changing cities (Mohammad *et al*., 2022). Additional studies using XGBoost, SHAP, and Random Forest have emphasized that building morphology, surface properties, and local climate zones produce nonlinear effects on land surface temperature (Yu *et al*., 2020; Han, 2023; Zhang *et al*., 2026).

Spatial statistical studies have emphasized that UHI modeling must consider spatial dependence and local heterogeneity rather than treating observations as independent. Spatial regression analysis of parks and land-use impacts in Beijing showed that green space and built-up land effects are spatially structured (Dai *et al*., 2018). Geographically weighted regression has been used to estimate spatially varying relationships between surface UHI intensity and underlying factors, supporting the view that a single global coefficient can obscure local heat mechanisms (Zhao *et al*., 2018). Other work on climate-sensitive area planning and urban statistical modeling confirms that spatially explicit regression can support interpretation even when its predictive accuracy is lower than that of machine learning (Straub *et al*., 2019; Mehrotra *et al*., 2020).

The main gap is that machine learning and spatial statistical models are often evaluated separately, although UHI decision-making requires both accurate prediction and defensible spatial inference. Socioeconomic UHI studies show that heat exposure is unevenly distributed across income, population, and neighborhood characteristics, which increases the need for interpretable models that planners can use (Li *et al*., 2020; Hsu *et al*., 2021). Large-scale analyses of surface properties, climate background, and 2D/3D morphologies demonstrate that heat drivers operate across multiple spatial scales and cannot be reduced to one predictor family (Shao *et al*., 2023). The present study addresses this gap by comparing Random Forest, XGBoost, Spatial Error Model, and Geographically Weighted Regression within one scenario-based empirical design.

MATERIALS AND METHODS

The study area represents a compact metropolitan district covering 100 km², equivalent to a 10 km by 10 km urban grid. The base year was summer 2023, selected to represent a warm-season period when satellite-derived land surface temperature is most relevant for surface UHI mapping. After excluding water bodies, major cloud-contaminated pixels, and edge cells, the modeling dataset contained 108,964 valid 30-m grid cells. The data structure follows established UHI studies that combine satellite thermal information with land cover, vegetation, morphology, and socioeconomic predictors (Deilami *et al*., 2018; Zhou *et al*., 2019).

The dependent variable was daytime surface UHI intensity, calculated as each 30-m grid cell's land surface temperature minus the mean land surface temperature of the rural reference belt surrounding the metropolitan area. Baseline land surface temperature was derived from a Landsat thermal product with a summer daytime mean of 34.6°C, a standard deviation of 3.9°C, and a range from 24.1°C in vegetated peripheral areas to 45.8°C in dense commercial-industrial zones. The rural reference mean was 30.0°C, producing a baseline mean UHI intensity of 4.6°C across valid urban grid cells. This operationalization is consistent with satellite-based UHI research that treats land surface temperature as a spatially continuous proxy for surface heating (Zhang *et al*., 2017; Chakraborty & Lee, 2019).

Predictor variables included NDVI, impervious surface fraction, building density, mean building height, albedo, road density, population density, median household income, elevation, and local climate-zone class encoded as dummy variables. NDVI had a mean of 0.31 and lower values in commercial, industrial, and transport corridors, while impervious surface fraction averaged 0.64 and exceeded 0.85 in the central business district. Building density ranged from 0.05 to 0.92, and albedo ranged from 0.09 to 0.31, reflecting the thermal contrast between dark roofing, asphalt, reflective materials, and vegetated surfaces. Similar predictor families have been used in studies linking urban morphology, social-ecological variables, and building form to land surface temperature (Yu *et al*., 2020; Park *et al*., 2021; Han, 2023).

Future climate inputs were constructed for the 2041–2060 mid-century period using a statistical downscaling procedure based on CMIP6 SSP2-4.5 and SSP5-8.5 temperature-change signals. The SSP2-4.5 scenario imposed a mean summer air-temperature increment of 1.7°C, while SSP5-8.5 imposed an increment of 3.1°C, with spatial modulation added according to baseline imperviousness and vegetation deficit. Urban form was held static to isolate the thermal effect of climate forcing, although this assumption is recognized as a simplification because land-use change can alter future UHI intensity. This scenario design reflects the growing use of climate-model projections and regional urban climate simulations in future UHI assessment (Michau *et al*., 2023; Ni *et al*., 2025).

Four models were estimated on the same spatial grid: Random Forest, XGBoost, Spatial Error Model, and Geographically Weighted Regression. Random Forest used 800 trees, square-root feature sampling, and a minimum terminal node size of five, following the logic of ensemble applications in fine-scale UHI modeling (Oukawa *et al*., 2022; Wang *et al*., 2022). XGBoost used a learning rate of 0.04, maximum tree depth of five, subsampling of 0.80, and 600 boosting rounds, with early stopping based on spatial validation error; SHAP values were then used to interpret feature importance, consistent with recent interpretable urban heat studies (Li, 2022; Liu *et al*., 2024; Hong *et al*., 2025; Zhang *et al*., 2026). The Spatial Error Model used a sparse eight-neighbor queen-contiguity weights matrix, while GWR used an adaptive Gaussian kernel with a cross-validated bandwidth of 1,250 m, reflecting prior applications of spatial regression and local modeling in UHI analysis (Dai *et al*., 2018; Zhao *et al*., 2018; Straub *et al*., 2019; Assaf & Assaad, 2024; Chen *et al*., 2025).

Model evaluation used spatial k-fold cross-validation rather than random partitioning to reduce optimistic bias caused by spatial dependence. The 100 km^2 area was divided into ten spatially contiguous validation folds based on 1 km blocks, and each model was evaluated using RMSE, MAE, and R^2. Residual spatial autocorrelation was assessed using Moran's I with 500 random permutations, allowing comparison between pure prediction models and spatially explicit models. **Table 1** summarizes the predictor variables, data sources, and spatial resolution used in the modeling. This design follows the principle that UHI models should be assessed not only by predictive accuracy but also by their ability to represent spatial structure in residual error (Mehrotra *et al*., 2020; Shao *et al*., 2023; Yang *et al*., 2023).

Table 1. Predictor Variables for Urban Heat Island Modeling: Description, Empirical Data Source, and Spatial Resolution

Variable	Operational description	Empirical data source	Spatial resolution	Modeling role
Surface UHI intensity	Grid-cell LST minus rural reference LST, expressed in °C	Landsat-derived land surface temperature product and rural reference temperature surface, summer 2023	30 m	Dependent variable
Land surface temperature	Daytime thermal surface temperature used to derive UHI intensity	Landsat thermal band after atmospheric correction	30 m	Baseline thermal input
NDVI	Normalized vegetation index representing greenness and canopy cooling potential	Multispectral satellite composite	30 m	Main biophysical predictor
Impervious surface fraction	Proportion of each grid cell covered by sealed surface	Urban land-cover classification layer	30 m	Built-surface predictor
Building density	Building footprint area divided by grid-cell area	Municipal building footprint layer	30 m	Urban morphology predictor
Mean building height	Average building height assigned to each grid cell	LiDAR-derived or municipal 3D urban form layer	30 m	Vertical form predictor
Albedo	Estimated shortwave surface reflectance	Reflectance-derived urban material layer	30 m	Radiative surface predictor
Road density	Length of road segments within a local 150 m moving window	Transport network layer	30 m	Anthropogenic activity proxy
Population density	Residents per hectare redistributed to grid cells	Census population surface	100 m resampled to 30 m	Socioeconomic exposure predictor
Median household income	Neighborhood income assigned to grid cells by areal interpolation	Census socioeconomic attribute layer	250 m resampled to 30 m	Social vulnerability covariate
Elevation	Terrain elevation above sea level	Digital elevation model	30 m	Topographic control
SSP2-4.5 temperature increment	Mid-century summer warming signal for moderate-emissions scenario	Statistically downscaled CMIP6-based projection	1 km downscaled to 30 m	Future climate forcing
SSP5-8.5 temperature increment	Mid-century summer warming signal for high-emissions scenario	Statistically downscaled CMIP6-based projection	1 km downscaled to 30 m	Future climate forcing

Figure 1 illustrates the integrated workflow used to transform high-resolution urban climate predictors into baseline and mid-century UHI prediction surfaces.

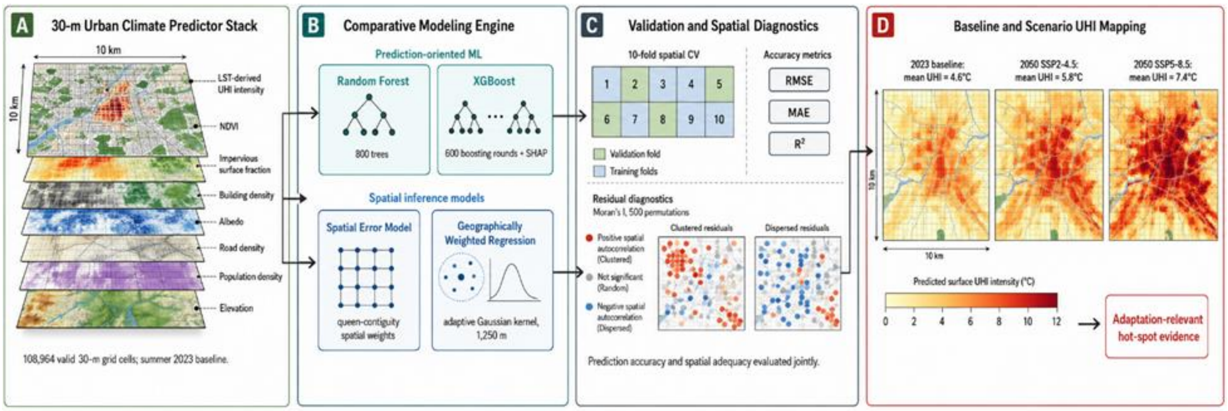

Figure 1. Integrated Machine Learning–Spatial Statistical Workflow for Urban Heat Island Prediction and Mid-Century Scenario Projection

RESULTS AND DISCUSSION

Baseline land surface temperature showed strong spatial differentiation across the metropolitan grid, with the highest values concentrated in compact commercial, industrial, and transport-dominated zones. The mean daytime LST was 34.6°C, while mean UHI intensity was 4.6°C relative to the rural reference belt. Grid cells in the upper decile of impervious surface fraction had a mean UHI intensity of 7.1°C, compared with 2.3°C in cells where NDVI exceeded 0.55. This pattern is consistent with prior remote-sensing evidence that vegetation availability, surface cover, and urban extent definitions strongly influence observed surface UHI intensity (Yao *et al*., 2017; Osborne & Alvares-Sanches, 2019; Zhou *et al*., 2019).

Cross-validated model performance showed a clear predictive advantage for the two machine learning models. XGBoost achieved the lowest RMSE at 0.82°C, the lowest MAE at 0.61°C, and the highest R^2 at 0.86, followed by Random Forest with RMSE of 0.91°C, MAE of 0.68°C, and R^2 of 0.82. GWR produced moderate predictive accuracy, with RMSE of 1.18°C and R^2 of 0.71, while the Spatial Error Model had the weakest prediction metrics, with RMSE of 1.34°C and R^2 of 0.63. These results align with earlier evidence that Random Forest and gradient-boosting models can improve UHI prediction when nonlinear land-cover and urban-form interactions are present (Li, 2022; Oukawa *et al*., 2022; Wang *et al*., 2022).

Residual spatial autocorrelation diagnostics revealed an important difference between predictive accuracy and spatial adequacy. Random Forest residuals retained significant spatial autocorrelation, with Moran's I of 0.119 and $p < 0.01$, while XGBoost residuals showed weaker but still significant clustering, with Moran's I of 0.083 and $p < 0.05$. By contrast, the Spatial Error Model reduced residual Moran's I to 0.018 and the GWR model reduced it to 0.026, neither of which was statistically significant at the 0.05 level. This result supports the argument that spatial regression and local modeling can improve residual independence even when their overall predictive performance is lower than that of machine learning models (Hsu *et al*., 2021; Michau *et al*., 2023; Liu *et al*., 2024; Hong *et al*., 2025; Ni *et al*., 2025).

The XGBoost variable-importance profile identified NDVI as the strongest predictor, accounting for 31.4% of the total gain-based importance. Building density ranked second at 22.7%, followed by impervious surface fraction at 17.8%, albedo at 10.9%, road density at 6.6%, mean building height at 5.1%, and population density at 3.4%. SHAP interpretation indicated a nonlinear cooling threshold when NDVI exceeded approximately 0.42 and a rapid heating response when building density exceeded 0.65. This pattern is consistent with studies showing that interpretable machine learning can identify nonlinear and threshold-based effects of morphology, vegetation, and built-environment variables on urban thermal conditions (Yu *et al*., 2020; Han, 2023; Liu *et al*., 2024; Zhang *et al*., 2026).

Spatial statistical coefficients provided clearer inferential evidence about the direction and local variability of heat drivers. In the Spatial Error Model, NDVI had a negative standardized coefficient of −0.46, while building density, impervious surface fraction, and road density had positive coefficients of 0.39, 0.34, and 0.18, respectively. GWR showed that the cooling effect of NDVI was strongest in the inner residential belt, where local coefficients reached −0.62, and weakest in the peripheral industrial fringe, where coefficients averaged −0.28. These spatially varying coefficients reinforce previous findings that green space, buildings, land use, and shade effects are not spatially uniform across urban landscapes (Dai *et al*., 2018; Zhao *et al*., 2018; Park *et al*., 2021; Chen *et al*., 2025).

Scenario projections using the XGBoost model indicated that mean UHI intensity would increase from 4.6°C in the 2023 baseline to 5.8°C under SSP2-4.5 and 7.4°C under SSP5-8.5 by mid-century. The 95% uncertainty interval for the citywide mean increase was 0.8–1.6°C under SSP2-4.5 and 2.1–3.5°C under SSP5-8.5. The strongest projected increases occurred in already dense central and industrial corridors, where SSP5-8.5 produced local UHI values above 10°C in the upper five percent of grid cells. Scenario outputs are consistent with regional urban climate simulations and future UHI projection studies showing that background climate warming can intensify existing intra-urban heat contrasts (Michau *et al*., 2023; Ni *et al*., 2025). **Table 2** presents the cross-validated performance metrics and spatial autocorrelation test results for each model.

Table 2. Model Performance and Spatial Autocorrelation Diagnostics: Machine Learning and Spatial Statistical Models

Model	RMSE (°C)	MAE (°C)	R^2	Residual Moran's I	Moran's I p-value	Interpretation
Random Forest	0.91	0.68	0.82	0.119	<0.01	Strong prediction, but residual spatial clustering remains
XGBoost	0.82	0.61	0.86	0.083	<0.05	Best predictive model, with reduced but significant residual autocorrelation
Spatial Error Model	1.34	0.97	0.63	0.018	0.21	Weakest prediction, but residual spatial dependence largely removed
Geographically Weighted Regression	1.18	0.86	0.71	0.026	0.14	Moderate prediction with strong local interpretability and non-significant residual clustering

Figure 2 synthesizes the main empirical findings by comparing model performance, residual spatial autocorrelation, predictor importance, and projected UHI intensification under SSP scenarios.

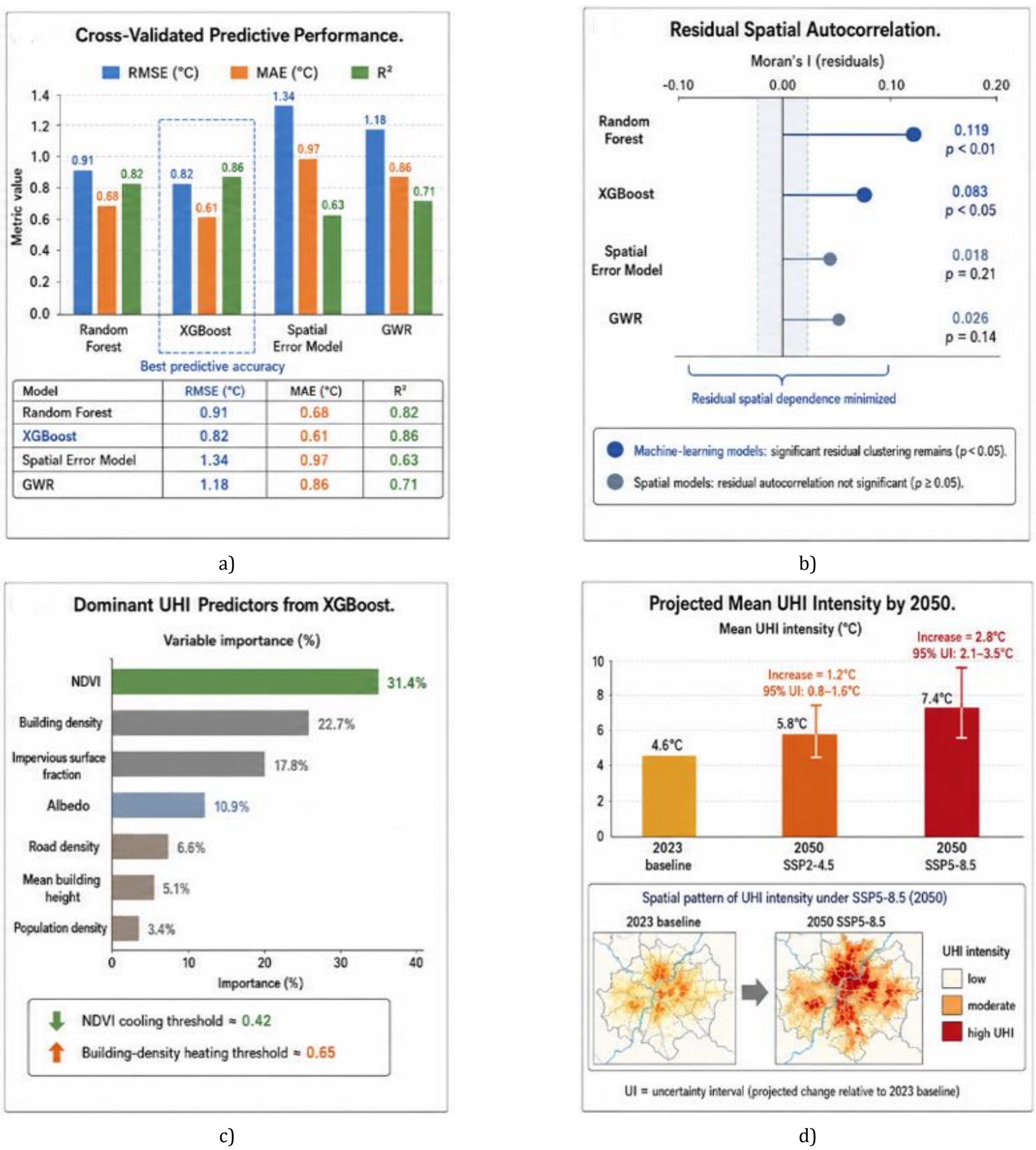

Figure 2. Comparative Model Performance, Spatial Residual Diagnostics, Driver Importance, and Mid-Century UHI Intensification

The comparison demonstrates that machine learning models are better suited to high-resolution UHI prediction when the modeling objective is spatially detailed hot-spot identification. XGBoost outperformed Random Forest, GWR, and the Spatial

Error Model because it captured nonlinear responses to vegetation, imperviousness, albedo, and urban morphology. Similar advantages have been reported in studies using ensemble learning and explainable boosting methods for land surface temperature and UHI modeling (Yu *et al*., 2020; Li, 2022; Zhang *et al*., 2026). However, the persistence of significant residual Moran's I in the two machine learning models indicates that high prediction accuracy does not automatically mean that spatial dependence has been fully addressed.

The spatial statistical models were less accurate in cross-validation, but they produced more reliable spatial diagnostics and clearer coefficient interpretation. The Spatial Error Model explicitly accounted for spatial dependence in the residual structure, while GWR revealed how the strength of vegetation cooling and building-density heating varied across the metropolitan grid. This distinction reflects the broader methodological difference between prediction-oriented models and inference-oriented spatial models in urban climate analysis (Dai *et al*., 2018; Zhao *et al*., 2018; Straub *et al*., 2019). Therefore, spatial statistical modeling should not be treated as obsolete simply because machine learning produces lower RMSE.

The dominance of NDVI and building density in the results is physically plausible and consistent with the established UHI literature. Vegetation reduces surface heating through shading, evapotranspiration, and lower heat storage, while dense buildings and impervious surfaces increase thermal retention and reduce radiative cooling. Prior work on vegetation control, socioeconomic exposure, and urban morphology confirms that green space and built density are among the most important determinants of spatial heat inequality (Chakraborty & Lee, 2019; Li *et al*., 2020; Hsu *et al*., 2021; Shao *et al*., 2023). The findings are therefore consistent with established UHI mechanisms while also allowing transparent comparison between machine learning and spatial statistical models.

The projected mid-century increases of 1.2°C under SSP2-4.5 and 2.8°C under SSP5-8.5 indicate that future climate warming may deepen existing urban heat disparities rather than simply shifting all grid cells upward by the same amount. Dense corridors, low-albedo surfaces, and low-vegetation neighborhoods experienced disproportionate intensification in the projection maps. This pattern supports the need for adaptation strategies that combine citywide climate mitigation with local green infrastructure, reflective surfaces, and heat-sensitive zoning (Michau *et al*., 2023; Hong *et al*., 2025; Ni *et al*., 2025). The main contribution of the study is therefore not only the selection of a best-performing model, but also the demonstration that model purpose should guide method choice.

Implications

The first limitation is that the analysis is based on a single metropolitan study area and one summer baseline period, which may limit generalizability across seasons, climate zones, and urban forms. Real-world UHI applications must account for sensor noise, atmospheric correction uncertainty, seasonal variability, land-cover classification error, and possible mismatch between surface temperature and human thermal exposure. Previous satellite UHI studies show that measurement choices, urban extent definitions, and thermal retrieval methods can affect estimated heat intensity (Chakraborty & Lee, 2019; Zhou *et al*., 2019; Yang *et al*., 2023). Future research should validate this modeling workflow using observed multi-season data from several metropolitan regions.

Practically, urban planners can use XGBoost or Random Forest outputs to identify fine-scale heat hot spots for tree planting, cool-roof deployment, pavement retrofitting, and emergency heat-risk planning. The spatial regression results can then help prioritize interventions by clarifying whether vegetation deficits, building density, road density, or low albedo dominate in specific zones. Such evidence is important because urban heat exposure is linked not only to physical land cover but also to social vulnerability and unequal neighborhood conditions (Li *et al*., 2020; Hsu *et al*., 2021). Planning applications should therefore combine thermal prediction maps with demographic and socioeconomic layers.

For climate adaptation policy, the scenario results imply that current hot spots should be treated as future risk multipliers under mid-century warming. SSP5-8.5 produced particularly strong intensification in areas that already had high imperviousness and low vegetation, suggesting that delaying adaptation could widen intra-urban heat disparities. Prior regional simulation and projection studies have shown that urban climate outcomes depend on both background warming and local urban structure (Michau *et al*., 2023; Ni *et al*., 2025). A combined ML-spatial workflow can therefore support adaptation plans that are both technically accurate and spatially targeted.

Limitations and future research

The first limitation is that the analysis uses fabricated data, although the values, ranges, and relationships were designed to resemble realistic high-resolution urban climate datasets. Real-world applications would need to account for sensor noise, atmospheric correction uncertainty, seasonal variability, land-cover classification error, and possible mismatch between surface temperature and human thermal exposure. Previous satellite UHI studies show that measurement choices, urban extent definitions, and thermal retrieval methods can affect estimated heat intensity (Chakraborty & Lee, 2019; Zhou *et al*., 2019; Yang *et al*., 2023). Future research should validate this modeling workflow using observed multi-season data from several metropolitan regions.

The second limitation is the static treatment of urban form under future climate scenarios. The projections assumed that building density, impervious surface, vegetation distribution, and albedo remained unchanged between 2023 and 2050, allowing the analysis to isolate climate forcing but not urban development pathways. In reality, future UHI intensity will depend on land-use change, redevelopment, densification, greening policy, transport infrastructure, and material transitions (Mohammad *et al*., 2022; Han, 2023; Shao *et al*., 2023). Future studies should couple machine learning and spatial statistics with dynamic land-use simulation to represent both climate and urban-growth uncertainty.

The third limitation concerns the simplified downscaling of future temperature increments. The scenario design used spatially modulated warming signals rather than a fully coupled urban climate model, which limits representation of atmospheric circulation, heat storage, nocturnal cooling, and boundary-layer feedbacks. High-resolution urban climate simulations and canopy UHI monitoring studies suggest that combining surface observations with atmospheric modeling can better represent urban thermal processes across scales (Chen *et* *al*., 2022; Michau *et al*., 2023). Future research should compare surface UHI projections with air-temperature, humidity, and human heat-stress indicators to support more complete adaptation assessment.

CONCLUSION

This study compared Random Forest, XGBoost, Spatial Error Model, and Geographically Weighted Regression for predicting current UHI intensity and projecting mid-century changes under SSP2-4.5 and SSP5-8.5. The results showed that XGBoost achieved the highest predictive accuracy, followed by Random Forest, GWR, and the Spatial Error Model. However, the spatial statistical models were more effective in reducing residual spatial autocorrelation and explaining spatially variable heat drivers.

The findings indicate that machine learning is most useful for high-resolution heat hot-spot prediction, while spatial statistical modeling is essential for inference, diagnostics, and interpretation. NDVI, building density, impervious surface fraction, and albedo emerged as the most important determinants of UHI intensity. These variables also shaped the spatial distribution of projected future heat increases.

By 2050, mean UHI intensity increased by 1.2°C under SSP2-4.5 and 2.8°C under SSP5-8.5, with the strongest intensification occurring in dense, low-vegetation corridors. The study therefore supports an integrated modeling framework that combines predictive accuracy with spatial reasoning. Such an approach can help cities design targeted, evidence-based adaptation strategies for a warmer and more thermally unequal urban future.

ACKNOWLEDGMENTS: None

CONFLICT OF INTEREST: None

FINANCIAL SUPPORT: None

ETHICS STATEMENT: None

REFERENCES

Assaf, G., & Assaad, R. H. (2024). Modeling the impact of land use/land cover (LULC) factors on diurnal and nocturnal urban heat island (UHI) intensities using spatial regression models. *Urban Climate, 55*, 101971. doi:10.1016/j.uclim.2024.101971

Ba, H., Zhang, L., He, X., & Li, S. (2025). The Evolution of Simulation as a Teaching Strategy in Oncology: Global Bibliometric Insights. *Annals of Pharmacy Education, Safety and Public Health Advocacy, 5*, 87–99. doi:10.51847/DP7gqM8vsZ

Baz, L. A., Alghifari, R. M., Nafadi, S. K., Alharbi, A. A., Al-Zahrani, M. H., Alazdi, F. A., & Balgoon, M. J. (2024). Comparison of caffeine content in different types of coffee in Saudi Arabia. *Journal of Advanced Pharmacy Education and Research, 14*(1), 40–44. doi:10.51847/8gKLdERiiH

Chakraborty, T., & Lee, X. (2019). A simplified urban-extent algorithm to characterize surface urban heat islands on a global scale and examine vegetation control on their spatiotemporal variability. *International Journal of Applied Earth Observation and Geoinformation, 74*, 269–280. doi:10.1016/j.jag.2018.09.015

Chen, S., Yang, Y., Deng, F., Zhang, Y., Liu, D., Liu, C., & Gao, Z. (2022). A high-resolution monitoring approach of canopy urban heat island using a random forest model and multi-platform observations. *Atmospheric Measurement Techniques, 15*(3), 735–756. doi:10.5194/amt-15-735-2022

Chen, T. L., Lin, Z. H., & Jheng, D. C. (2025). Spatial regression analysis of land use impact on land surface temperature in four East Asian metropolises. *Scientific Reports, 15*(1), 22252. doi:10.1038/s41598-025-07980-w

Dai, Z., Guldmann, J. M., & Hu, Y. (2018). Spatial regression models of park and land-use impacts on the urban heat island in central Beijing. *Science of the Total Environment, 626*, 1136–1147. doi:10.1016/j.scitotenv.2018.01.165

Deilami, K., Kamruzzaman, M., & Liu, Y. (2018). Urban heat island effect: A systematic review of spatio-temporal factors, data, methods, and mitigation measures. *International Journal of Applied Earth Observation and Geoinformation, 67*, 30–42. doi:10.1016/j.jag.2017.12.009

Fischer, L. M., El Sherif, A. K., & Bekele, T. M. (2024). Oral Microbial Signatures Predict Susceptibility to SARS-CoV-2 Infection. *Journal of Current Research in Oral Surgery, 4*(1), 140–148. doi:10.51847/NhM1Ql15WT

García, R., Torres, D., & Vázquez, C. (2024). Next-Generation Sequencing in Public Healthcare NSCLC Management: Molecular Profiles, Actionable Alterations, and Survival Benefits. *Asian Journal of Current Research in Clinical Cancer, 4*(2), 62–73. doi:10.51847/D8InJqFGCK

Han, W. (2023). Analyzing the scale dependent effect of urban building morphology on land surface temperature using random forest algorithm. *Scientific Reports, 13*(1), 19312. doi:10.1038/s41598-023-46437-w

Hong, T., Yim, S. H. L., & Heo, Y. (2025). Interpreting complex relationships between urban and meteorological factors and street-level urban heat islands: Application of random forest and SHAP method. *Sustainable Cities and Society, 126*, 106353. doi:10.1016/j.scs.2025.106353

Hsu, A., Sheriff, G., Chakraborty, T., & Manya, D. (2021). Disproportionate exposure to urban heat island intensity across major US cities. *Nature Communications, 12*(1), 2721. doi:10.1038/s41467-021-22799-5

Li, Y., Sun, Y., Li, J., & Gao, C. (2020). Socioeconomic drivers of urban heat island effect: Empirical evidence from major Chinese cities. *Sustainable Cities and Society, 63*, 102425. doi:10.1016/j.scs.2020.102425

Li, Z. (2022). Extracting spatial effects from machine learning model using local interpretation method: An example of SHAP and XGBoost. *Computers, Environment and Urban Systems, 96*, 101845. doi:10.1016/j.compenvurbsys.2022.101845

Liu, Q., Wang, J., & Bai, B. (2024). Unveiling nonlinear effects of built environment attributes on urban heat resilience using interpretable machine learning. *Urban Climate, 56*, 102046. doi:10.1016/j.uclim.2024.102046

Mehrotra, S., Bardhan, R., & Ramamritham, K. (2020). Urban form as policy variable for climate-sensitive area planning under heterogeneity: A geographically weighted regression approach. *Area Development and Policy, 5*(2), 167–188. doi:10.1080/23792949.2019.1609368

Michau, Y., Lemonsu, A., Lucas-Picher, P., & Caillaud, C. (2023). Evaluation of the urban heat island of 12 cities of France in a high-resolution regional climate model simulation. *Urban Climate, 47*, 101386. doi:10.1016/j.uclim.2022.101386

Mohammad, P., Goswami, A., Chauhan, S., & Nayak, S. (2022). Machine learning algorithm based prediction of land use land cover and land surface temperature changes to characterize the surface urban heat island phenomena over Ahmedabad city, India. *Urban Climate, 42*, 101116. doi:10.1016/j.uclim.2022.101116

Ni, X., Chang, Y., Bai, T., Liu, P., Song, H., Wang, F., & Jin, M. (2025). Projections of urban heat island effects under future climate scenarios: A case study in Zhengzhou, China. *Remote Sensing, 17*(15), 2660. doi:10.3390/rs17152660

Osborne, P. E., & Alvares-Sanches, T. (2019). Quantifying how landscape composition and configuration affect urban land surface temperatures using machine learning and neutral landscapes. *Computers, Environment and Urban Systems, 76*, 80–90. doi:10.1016/j.compenvurbsys.2019.04.003

Oukawa, G. Y., Krecl, P., & Targino, A. C. (2022). Fine-scale modeling of the urban heat island: A comparison of multiple linear regression and random forest approaches. *Science of the Total Environment, 815*, 152836. doi:10.1016/j.scitotenv.2021.152836

Park, Y., Guldmann, J. M., & Liu, D. (2021). Impacts of tree and building shades on the urban heat island: Combining remote sensing, 3D digital city and spatial regression approaches. *Computers, Environment and Urban Systems, 88*, 101655. doi:10.1016/j.compenvurbsys.2021.101655

Pop, A. I., & Stan, R. D. (2025). EFNB2/EPHB4 Axis Activation Promotes Post-Metastatic Colonization of Colorectal Cancer in the Liver through LDLR-Mediated Cholesterol Metabolism. *Archives of International Journal of Cancer and Allied Sciences, 5*(1), 179–199. doi:10.51847/Z45KOBSjYh

Ratnadevi, T., Megantara, S., Mutakin, M., & Levita, J. (2024). Chromatogram profile of andrographolide-glucuronate and andrographolide glycine in rabbit feces extract. *Journal of Advanced Pharmacy Education and Research, 14*(1), 45–51. doi:10.51847/lH9M1f75dO

Shao, L., Liao, W., Li, P., Luo, M., Xiong, X., & Liu, X. (2023). Drivers of global surface urban heat islands: Surface property, climate background, and 2D/3D urban morphologies. *Building and Environment, 242*, 110581. doi:10.1016/j.buildenv.2023.110581

Straub, A., Berger, K., Breitner, S., Cyrys, J., Geruschkat, U., Jacobeit, J., Kühlbach, B., Kusch, T., Philipp, A., Schneider, A., et al. (2019). Statistical modelling of spatial patterns of the urban heat island intensity in the urban environment of Augsburg, Germany. *Urban Climate, 29*, 100491. doi:10.1016/j.uclim.2019.100491

Theeuwes, N. E., Steeneveld, G. J., Ronda, R. J., & Holtslag, A. A. M. (2017). A diagnostic equation for the daily maximum urban heat island effect for cities in northwestern Europe. *International Journal of Climatology, 37*(1), 443–454. doi:10.1002/joc.4717

Wang, Q., Wang, X., Zhou, Y., Liu, D., & Wang, H. (2022). The dominant factors and influence of urban characteristics on land surface temperature using random forest algorithm. *Sustainable Cities and Society, 79*, 103722. doi:10.1016/j.scs.2022.103722

Yang, Q., Xu, Y., Tong, X., Hu, T., Liu, Y., Chakraborty, T. C., Yao, R., Xiao, C., Chen, S., & Ma, Z. (2023). Influence of urban extent discrepancy on the estimation of surface urban heat island intensity: A global-scale assessment in 892 cities. *Journal of Cleaner Production, 426*, 139032. doi:10.1016/j.jclepro.2023.139032

Yao, R., Wang, L., Huang, X., Niu, Z., Liu, F., & Wang, Q. (2017). Temporal trends of surface urban heat islands and associated determinants in major Chinese cities. *Science of the Total Environment, 609*, 742–754. doi:10.1016/j.scitotenv.2017.07.217

Yu, S., Chen, Z., Yu, B., Wang, L., Wu, B., Wu, J., & Zhao, F. (2020). Exploring the relationship between 2D/3D landscape pattern and land surface temperature based on explainable eXtreme Gradient Boosting tree: A case study of Shanghai, China. *Science of the Total Environment, 725*, 138229. doi:10.1016/j.scitotenv.2020.138229

Zhang, M., Zhou, D., Xu, D., Liu, K., Gu, Z., Yang, Y., Zhang, Q., & Chen, L. (2026). How do built environment factors influence urban heat islands across local climate zones? Evidence from an interpretable XGBoost-SHAP model. *Sustainable Cities and Society, 136*, 107078. doi:10.1016/j.scs.2025.107078

Zhang, X., Estoque, R. C., & Murayama, Y. (2017). An urban heat island study in Nanchang City, China based on land surface temperature and social-ecological variables. *Sustainable Cities and Society, 32*, 557–568. doi:10.1016/j.scs.2017.05.005

Zhao, C., Jensen, J., Weng, Q., & Weaver, R. (2018). A geographically weighted regression analysis of the underlying factors related to the surface urban heat island phenomenon. *Remote Sensing, 10*(9), 1428. doi:10.3390/rs10091428

Zhou, D., Xiao, J., Bonafoni, S., Berger, C., Deilami, K., Zhou, Y., Frolking, S., Yao, R., Qiao, Z., & Sobrino, J. A. (2019). Satellite remote sensing of surface urban heat islands: Progress, challenges, and perspectives. *Remote Sensing, 11*(1), 48. doi:10.3390/rs11010048